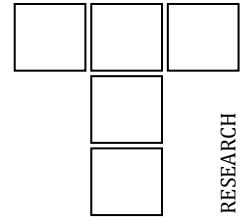


DOI: 10.24874/ti.1787.11.24.11

Tribology in Industry

www.tribology.rs



Spectroscopic, Diagnostics, and Surface Modification of Stainless Steel Doped with Ti Plasma Produced by DC Magnetron Sputtering and Used in Biomedical Applications

Mustafa A. Mahmood^{a,*}, Riyam Adnan Hammudi^b


^aDepartment of medical physics, College of sciences, Al-karkh University of science, Baghdad, Iraq,

^bDepartment of Physiology and Medical Physics, College of Medicine, Wasit University, Wasit -Al Kut 52001, Iraq.

Keywords:

304 stainless steel
Platinum doping
Characterisation
Biomedical applications

* Corresponding author:

Mustafa A. Mahmood 
E-mail:
mustafa.a.mahmood@kus.edu.iq

Received: 19 September 2024

Revised: 24 October 2024

Accepted: 27 November 2024



ABSTRACT

Significant developments have been made in the plasma spray process in recent years. In this process, high-quality, denser coatings can be produced. In the current study, titanium films with ~3 nm thickness were developed on 304 stainless steel bars by DC magnetron sputtering technique. It was determined that the developed titanium doping has good properties. 304 stainless steels doped with titania characterised with XRD confirmed the TiO₂ coating. Also, they showed that the broadening of the peaks was due to residual stresses in the substrate, present in the austenite phase of the substrate and a possible combination of fine grain and residual stresses in the TiO₂ layer. SEM-EDS analyses confirm the roughness of the surface and elemental composition of stain steel doping with titania with 4.5 eV peak and 6.5eV peak. FTIR spectra also specify the Ti-O and Fe-O bonds in the prepared alloy. Topological modifications of 304 stainless steel surfaces caused by TiO₂ plasma treatment can be quantified in terms of roughness by AFM analysis. It indicated that the rough surface was obtained due to the doping process. The biological application of the prepared alloy sample was tested using the immersion technique. The doped sample was subjected to a bioactivity test. The cytotoxicity results demonstrate a significant cytotoxic effect on CHO cells, which could be attributed to the high concentration of metal ions produced by the material's biocorrosion, which causes the culture medium's pH to change quickly, as indicated by a change in colour.

© 2024 Published by Faculty of Engineering

1. INTRODUCTION

Coatings obtained by Plasma processes are among the hardest [1-2]. The Magnetron Sputtering technique has a high deposition rate,

low working pressure, low discharge voltage and a non-uniform thickness of the obtained layer. This technique is commonly used in producing coatings subjected to high friction and wear [2]. Due to the characteristics of the

process, the layers obtained by the plasma method may have high residual stresses. Plasma gas consists of ions, free electrons, and neutral atoms. When the electrons of a plasma have a significantly higher velocity distribution than the ions, the plasma is called an "unstable plasma." Examples of such plasmas occur in fluorescent lamps, chemical reactors, etc. Unstable plasmas occur at low pressures (< 1 Pa), high voltages, low currents, and gas temperatures. While unstable plasmas are widespread, stable or thermal plasmas are important in plasma spray coating technology [3].

Plasma spray coatings provide significant advantages: Coating and substrate materials can be selected and combined independently. The composition, configuration and properties of plasma spray coating layers can be changed widely and optimised for specific applications. Small or large parts can be coated with plasma spraying [4]. In the plasma spraying process, highly advanced technology can be used to increase the economic performance and quality of the coating. The plasma spray process can be easily integrated between the manufacturing stages in part production. In particular, the high process temperature of the plasma spray method allows working with metals and alloys with high melting points. In addition, the advantage of the method is that it can be used in harsh environments and vacuum environments. All materials produced in powder form and with specific grain sizes are successfully used in this process. In addition to coating materials, the plasma spray method repairs areas damaged by wear, heating or corrosion [5].

Traditional uses of titanium dioxide include analysing and exploiting its biological and mechanical catalytic properties [6]. However, recent studies define it as a biocompatible material, which, combined with other compounds, increases its mechanical and anticorrosive properties and can have great biomedical applications. It can be said that all titanium prostheses have a layer of titanium on their surface since it is formed naturally and interacts with the medium [6-7]. In the studies of Li et al. [8], it was concluded that TiO₂

coatings have good mechanical properties. On the other hand, Fu et al. [9] reports suggest using TiO₂ coatings on Hydroxyapatite coating (HA) due to its high corrosion resistance.

This study aims to characterise the microstructure and mechanical properties of coatings produced by applying direct and intermediate coatings to titanium metal surfaces using the plasma spray method and to determine and characterise the bioactivity properties of the obtained coatings in artificial body fluids.

2. MATERIALS AND METHOD

2.1 Methodology

Samples of 304 steel (Triton Alloys Inc., India) were cut, the chemical composition shown in Table 1, measuring 3x13x0.2 mm³ on a low-speed diamond blade cutter, which was mechanically polished to a mirror finish on both sides. 304 steel is widely used industrially, is austenitic and may present martensite induced by plastic deformation [10]. The coatings were made on DC Magnetron Sputtering (Hind Hi Vacuum Systems, Model - Smart Coat 3.0 RF/DC Sputtering System) method [11]. The samples were coated under high vacuum conditions in a mixed atmosphere of Argon and Nitrogen at 200 °C. Cleaning was carried out with isopropyl alcohol and acetone. During the production of the films, parameters that could affect the coating, such as substrate temperature (R_T = 200°C), coating pressure (30 mTorr), rotation speed (3 rpm), and thickness 3(mm), Substrate RF bias -30V, Magnetron power 2x250RF were kept constant. The thickness of the films was monitored with the thickness gauge inside during the growth period. They were then rinsed with water and dried with pressurised air. They were taken to a convection oven at 120°C. In the reactor, an ion bombardment with argon was carried out on the samples to remove the oxide layer present. When the samples were removed, their thicknesses were confirmed using a Dektak 150 profilometer.

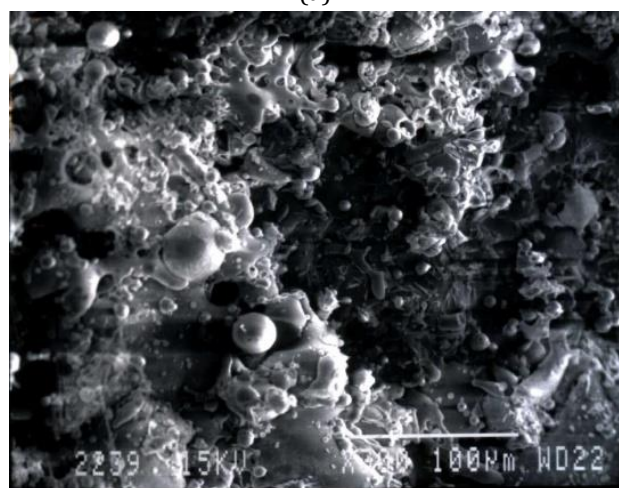
Table 1. Chemical composition results for 304 stainless steels.

C	Si	Mn	S	P	Ni	Cr	Mo	Al	Cu	V
0.031	0.529	1.562	0.026	0.025	8.629	18.96	0.108	0.006	0.154	0.956

Below in Figure 1(a), the photographs of the Ti interlayer and 304 stainless steel monolayers obtained by DC sputtering technique and the secondary electron image obtained from the coating surface at an angle of 10° after plasma spray coating is given in Figure 1b.



(a)



(b)

Fig. 1. (a) 304 substrates with titanium film, (b) SEM image of a top view.

2.2 Coating Characterization

The techniques used for the characterisation of coatings are briefly described below. Characterisation with the X-ray diffraction (XRD) technique using Bruker d8 with $\text{CuK}\alpha$ radiation with 2θ changing between 10 and 100° allows the presence of residual elastic stresses to be determined. If the width at half the height of peak intensity in the XRD spectrum is more significant than 0.1° , there is a β widening that may be due to residual stresses in the lattice ($\beta\tau$) or grain size (TG) less than 1mm ($\beta\tau$), [12]. If the grain size of the sample is much larger than 1mm, the widening of the peaks can then be associated with residual elastic deformation. In addition, the characterisation is presented through the use of

Automatic atomic force microscopy (AFM) (Park FX40) and scanning electron microscopy-energy dispersive x-ray spectroscopy (SEM-EDS) JEOL JSM 5910LV model equipment, seeking to establish the relationship between residual stresses and the microstructure. FTIR Spectrometer (Thermo Fisher Scientific Nicolet™ iS50) is used to determine the information about the molecular vibrational modes of the atomic bonds of the material under study. Profilometry measurements were made to obtain information on the thickness of the synthesised films. These measurements were made in a Veeco Dektak 150 profilometer with 100, 300 and 600 μm scans.

2.3 Cytotoxicity analysis

The cytotoxic potential of the 304-steel doped with TiO_2 alloy was evaluated using the MTT reduction technique (3-(4,5-dimethylthiazol-2-yl)-2,5-diphenyl tetrazole bromide). This method allows for determining the percentage of cell viability, considering the integrity of the membrane.

The cytotoxic effects were evaluated on the corrosion products of the porous material. This quantification was carried out indirectly using Chinese hamster ovary epithelial cells (CHO-K1), cultured in RPMI 1640 culture medium, supplemented with fetal bovine serum (FBS), in a 96-well culture dish incubated for 24 hours. Before subjecting the culture to the different treatments, a CHO-K1 cell line with a confluence of 90% was taken. The cells attached to the culture flask were resuspended and stained with trypan blue to be counted. Trypan blue is a selective staining dye that allows for the observation of the difference between viable and non-viable cells since living cells have intact cell membranes that exclude certain dyes, so living cells have clear cytoplasm. In contrast, non-viable cells are observed with blue cytoplasm.

10 μL of the cell suspension was mixed in an Eppendorf tube with 10 μL of trypan blue solution (stock at a concentration of 0.4%). 10 μL of this new suspension was counted in the Neubauer chamber. The percentage of viable cells was calculated following equation 1.

$$\% \text{ Cell Viability} = \frac{\text{Viable Cells} \times \text{mL of Aliquot}}{\text{Total Cells} \times \text{mL of Aliquot}} \times 100 \quad (1)$$

After 24 hours, the culture medium was discarded from each of the wells and replaced with medium supplemented with 10% FBS and 50 µL of the aqueous extract resulting from the corrosion of the two surface configurations. The quantities of the components used for inoculating the plates are described in Table 2. The starting point was a cell suspension viability of 94%. Additionally, considering that this type of cell grows in a monolayer, the growth and adherence on the two types of surfaces were evaluated.

Table 2. A number of components used for plate inoculation.

Component	Amount per well	Quantity per Plate (96x)
CHO-K1 cells	5 µL	480 µL
Culture medium	79 µL	7584 µL
Serum	4 µL	384 µL
Antibiotic	1 µL	96 µL
Extract	1 µL	96 µL
Total volume	90 µL	8640 µL

After 48 hours of exposure to the treatment, a colourimetric test was performed to estimate the percentage of viable cells. 100 µL of MTT were added to each well. This technique allows quantifying the reduction of tetrazolium salts that cause the formation of an insoluble precipitate of intense colour, known as Formazan, by the action of metabolically active cells to form violet crystals. The reduction reaction was carried out for approximately three hours. The formed crystals were resuspended by adding 100 µL of acid isopropanol in the following proportions: 89.2% isopropanol, 10% triton and 0.8% HCl. Crystal formation was quantified by recording the changes in absorbance of the samples at a wavelength of 570 nm with an ELISA plate reader coupled with the Elico SL 159 Model spectrophotometer. The results in terms of viability were found following equation 2.

$$\% \text{ Viability} = \frac{\text{Treatment Average} - \text{Blank Average}}{\text{Negative Control Average} - \text{Blank Average}} \times 100 \quad (2)$$

Where:

- Treatment average: Average absorbance obtained with the treatment.
- Blank average: Average absorbance obtained from the blank
- Negative control average: Absorbance obtained from the negative control

3. RESULTS

3.1 Characterization of the prepared metallic surfaces

3.1.1 Top view of plasma spray coating:

Stainless steel coating-substrate interface and coating-interlayer-substrate interface cross-sections were examined using backscattered electrons. The images obtained show an average of 110µm of coating on the steel substrate surface for direct coating, an average of 20µm in intermediate coating application and intermediate coating, and an average of 80µm of Titanium coating (Figure 2 (i) & (ii)). No reaction formation could be determined with the characterisation technique used in the interfaces with and without intermediate coating. This can be expressed as an indication of the formation of a mechanical bond at the coating-substrate interface [12].

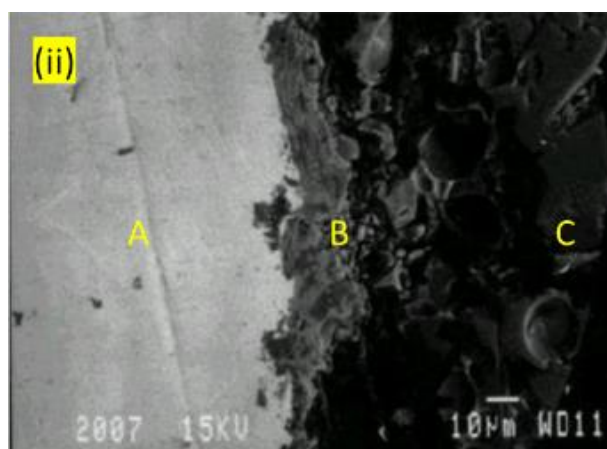
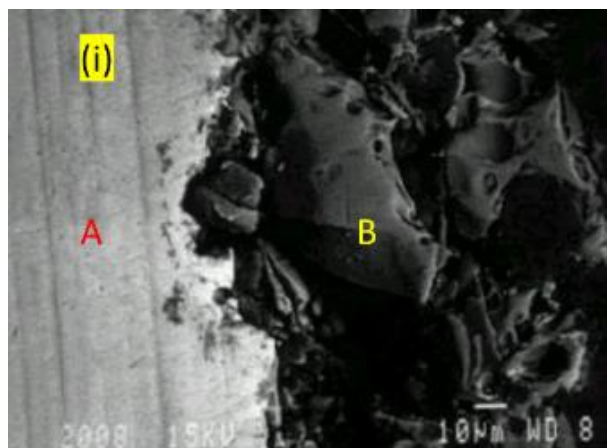


Fig. 2. (i) Substrate (A)-304 Stainless steel (B) coating interface; (ii) (A)-Intermediate coating (B)-304 Stainless steel (C) interface.

3.1.2 SEM-EDS analysis

The SEM micrographs taken of the samples after the metallographic attack in Figure 3a,b and c confirm that the material is 304 stainless steel, according to the distribution of the austenite. In addition, it can be seen that the material

presents specific amounts of non-metallic inclusions (impurities). In the three samples (Figure 3), it can be determined that the number of impurities varies depending on the cross-section of the material that is analysed since these samples were taken randomly from the different cuts made to the material.

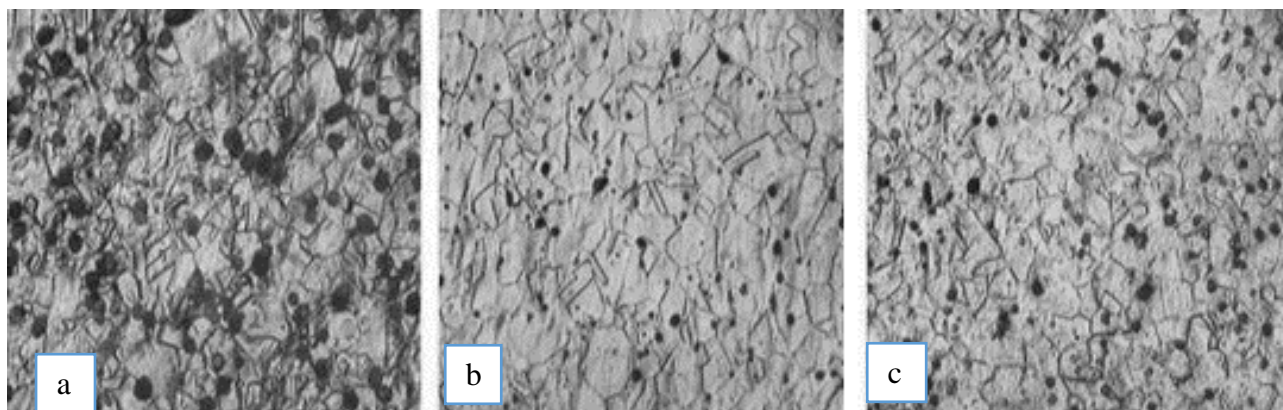


Fig. 3. SEM analysis of three 304 substrates at a resolution of 200X magnification.

The analysis of the composition of the 304 stainless steel coated with titanium film by EDS is presented in Figure 4a and b. As can be seen in the selected section, the substrate surface has a non-uniform appearance and contains Ti, O, Si, Cr, and Fe (~81% total). The spectrum shows a strong Ti signal around 4.4 eV, confirming that the layer formed is mainly composed of titania

and a peak around 6.4 eV corresponding to the presence of iron is observed [13]. The sample preparation for analysis probably fractured the structure, exposing the magnetite to the surface. An important characteristic is that the peaks associated with the steel substrate are less intense than those associated with Titanium [13].

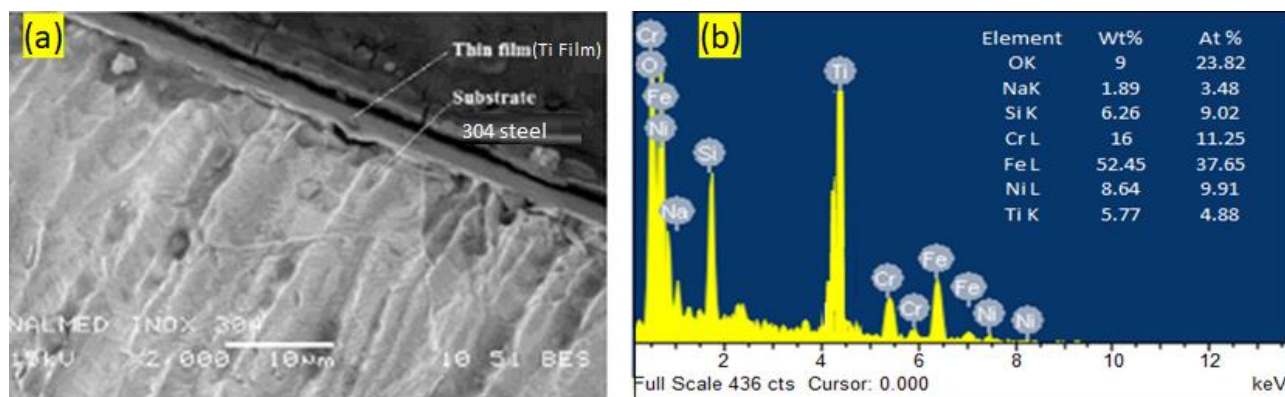


Fig. 4. SEM-EDS spectra of 304 stainless steel doped with titanium film.

3.1.3 Atomic Force Microscopy (AFM) analysis

Topological modifications of 304 stainless steel surfaces caused by TiO₂ plasma treatment can be quantified in terms of roughness by AFM, and the resulting images are given in Figure 5a. Figure 5 is an AFM image taken on top of the layer, where some holes are noticeable. The coating copied the shape of the slip bands on the substrate

surface, as shown in Figure 5b. AFM image analysis has been a valuable tool for measuring this phenomenon [14]. It was described in the form of two parameters: the mean roughness (Rq) and the distance between the top and bottom of the protuberances (Rmax). These parameters were calculated for the initial samples and those subjected to 1000 and 5000s plasma treatment. The data are shown in Table 3.

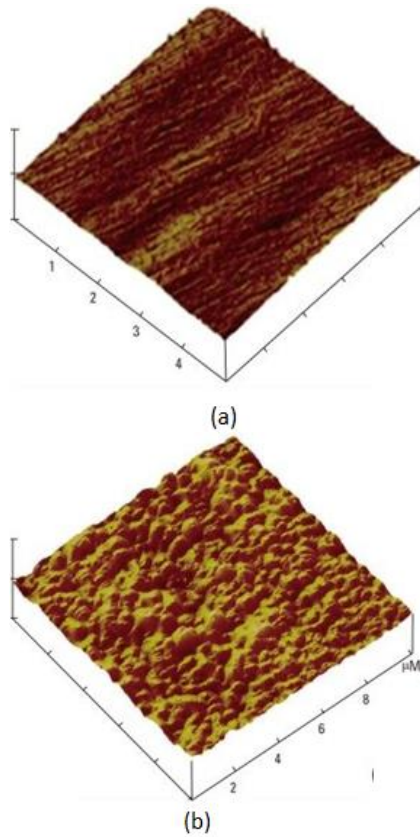


Fig. 5. Evolution of the 304 stainless steel surfaces as a function of plasma treatment at 5000s and 1000s.

The initial 304 stainless steel sample presented a relatively flat surface whose roughness increased after plasma treatment, with an increase in the values of R_q and R_{max} . Figure 5 shows the evolution of the 304 stainless steel roughness as the plasma treatment period increased.

Table 3. R_q and R_{max} data of the samples as a function of treatment time.

Sample	Time (s)	R_q (\AA)	R_{max} (\AA)
304 stainless steel with titanium coating	0	28	159
	1000	214	1434
	5000	146	1153

3.1.4 XRD spectrum of the TiO₂-coated 304 stainless steel

Figure 6 shows the XRD spectrum of the layer-coating system, measured on the layer, where peaks corresponding to the austenite phase (111, 220, 311); to TiO₂ (111, 200) and to the martensite phase (200, 211) appear; which confirms the result of the magnetic test. The position of the TiO₂ peaks (111), (200) and (311) coincides with results reported in the literature, where TiO₂ has been used as a coating [9]. The peaks were numbered from left to right with letters from 1 to 8.

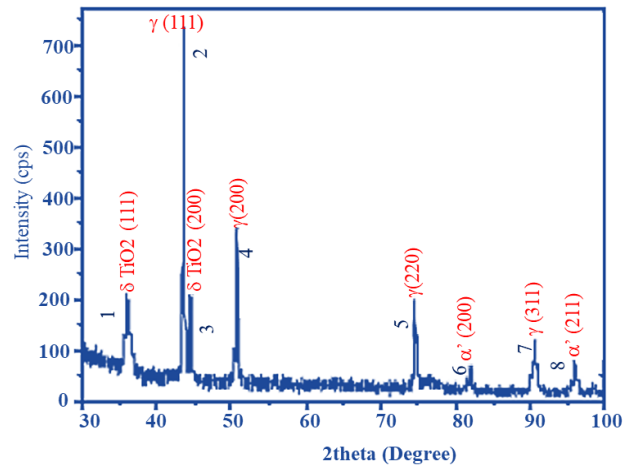


Fig. 6. XRD spectra of TiO₂ coated 304 stainless steel sample.

In the low angle zone, a typical background of an amorphous material is noted due to the sample holder, which is affected by the incident beam due to the small dimensions of the examined sheet, $3 \times 13 \times 0.2 \text{ mm}^3$. The XRD peaks in Figure 6 are broadened β relative to the instrumental width since the width at half height is more significant than 0.1° [4]. The (111) texture coefficient found for the TiO₂ layer [16] was 0.7649, since $I_{111} = 194.644$ and $I_{200} = 59.830$, where I is the area under the peak, adjusted with the 'Peak Fit' software. This means that the (111) texture is 76.5% of the total of (111) and (200). The results are summarised in Table 4.

A heat treatment was performed to analyse the XRD peaks of austenite to obtain 100% austenite and compare with the peaks previously obtained for 304 steels. Figure 7 presents the two spectra obtained, superimposed for comparison purposes, and the values reported in the literature for austenite without broadening.

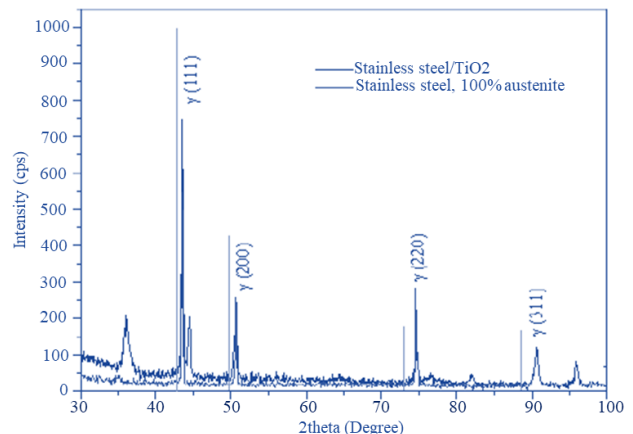


Fig. 7. Comparison of XRD spectrum of the 304/TiO₂ with a substrate with 100% austenite and with some values reported in the literature [15].

Table 4. Residual elastic deformation of the peaks corresponding to the substrate, assuming that it is due to the residual stresses of the network, i.e., $b=b_e$.

Peak Number	Diffraction Planes	Measured Position (2 θ)	Reported Standard Position	Amplitude (Counts per sec)	Width at half height ($^\circ$)	Width at half height (rad)	Peak broadening $b=b_e$ (rad)	Integral (Area under peak)	Grating def. per sph. Res.
2	g(111)	44.04	42.75	671.23	0.11	1.80×10^{-3}	0.80×10^{-3}	213.51	$5.10E-04$
4	g(200)	51.21	49.78	189.1	0.17	2.76×10^{-3}	1.76×10^{-3}	90.81	$9.30E-04$
5	g(220)	75.45	73.06	87.51	0.2	3.26×10^{-3}	2.26×10^{-3}	48.9	$7.40E-04$
6	a(200)	82.72	82.01	27.1	0.49	8.08×10^{-3}	7.08×10^{-3}	35.82	$2.04E-03$
7	g(311)	91.51	88.54	101.62	0.26	4.35×10^{-3}	3.35×10^{-3}	77.54	$8.30E-04$
8	a(211)	96.86	-	62.4	0.22	3.68×10^{-3}	2.68×10^{-3}	40.16	$6.00E-04$

To check whether the peak broadening recorded in Table 4 is due to TG, the value of J was used to calculate it, i.e. $b=b_t$ was taken. The results are summarised in Table 5. It is observed that the TG associated with J would be in magnitudes lower than $0.2 \mu\text{m}$. Since the TG for steel varies

between 10 and $60 \mu\text{m}$, the broadening of the XRD peaks is due to some additional effect, i.e. residual stresses. The grain size was not calculated exactly because its impact on the residual stresses was quickly discarded for being so far from the critical value of $1 \mu\text{m}$.

Table 5. TG grain size for steel assumes that peak broadening is due to a TG less than $1 \mu\text{m}$, i.e., i.e., $b=b_t$.

Peak Number	Diffraction Planes	Broadening of $\pi, \beta\tau$ (rad)	TG (m)	TG (μm)
2	g(111)	0.80×10^{-3}	1.87×10^{-7}	0.189
4	g(200)	1.76×10^{-3}	8.73×10^{-8}	0.088
5	g(220)	2.26×10^{-3}	$7.72E \times 10^{-8}$	0.078
6	a(200)	7.08×10^{-3}	2.60×10^{-8}	0.026
7	g(311)	3.35×10^{-3}	5.89×10^{-8}	0.06
8	a(211)	2.68×10^{-3}	7.73×10^{-8}	0.078

Table 5 shows that the spectrum peaks obtained for 100% austenite in the steel sample do not have broadening. This spectrum is superimposed with the spectrum obtained for the 304/TiO₂ samples. It is noted that the peaks associated with the austenite of the coated sample coincide precisely with the austenite peaks present in the sample with 100% austenite, confirming the interpretation made on the results of the TiO₂ coated sheet.

3.1.5 Analysis of the XRD Peaks for the Substrate 304 Steel

The elastic residual strain (ϵ) in the substrate was calculated [11] assuming that β is due only to residual stresses in the peaks obtained, i.e. $\beta=\beta \epsilon$. The results are presented in Table 4, where the peak position reported in the literature for each peak when no residual stresses are also indicated. This table shows that all the peaks are broadened since they present values greater than 0.1° . To determine the broadening $\beta \tau$, 0.1° was subtracted from each peak width value and the residual deformation ϵ was determined [11], which is presented in the

same table, being of the order of 10^{-4} for austenite and martensite in the (211) plane and 10^{-3} for martensite in the (200) plane.

3.1.6 Infrared Spectrum Characteristics

Based on the characterisation results, FTIR for the 304/TiO₂ metal spectrum was obtained; this spectrum is shown in Figure 8.

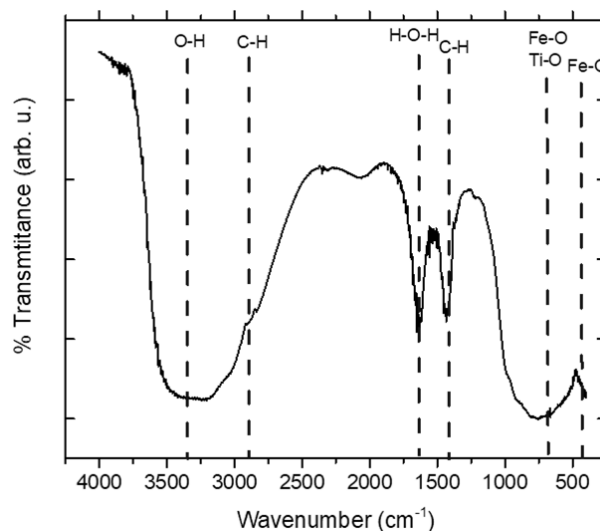


Fig. 8. FT IR spectra of 304 steel doped with TiO₂ plasma.

Indication of -OH stretching groups at wave numbers in the absorption group of 3383.14 cm⁻¹ comes from ethanol as a solvent for making FeTiO₂—indicating the presence of the -C-H group at wave numbers of 2876.30 cm⁻¹. The C-H group is at wave numbers of 1425.40 cm⁻¹. Wave numbers <700 cm⁻¹ with high absorption intensity come from the Fe-O and O-Ti-O metal bonds [17].

3.1.7 Surface Roughness

Metal surfaces and coating average surface roughness values (Ra) before and after coating were determined with a surface roughness measuring device perthometer (Salbro Engineers, India). Stainless steel surface roughness value (after sandblasting) Ra: 7.4 μm, surface roughness value after intermediate coating application Ra: 9.05 μm, surface roughness value after Titanium coating on the intermediate layer applied surface Ra: 9.92 μm, surface roughness value of Titanium coating applied directly to the metal surface without intermediate coating was found as Ra: 12.79 μm. The effect of surface roughness on mechanical properties is examined in the discussion section [18-20].

3.2 Cytotoxicity analysis

After 48 hours of incubation of the culture with fragments of approximately 0.1 g of the alloy, a visual inspection was performed, and it was observed that the wells cultured with Mg had a yellow colour different from the colour of the control wells on the plate. In addition, it was identified that in the initial state, the cells in the wells cultured with Iron/Ti were not adhered to, which gives an initial sample of the negative effect of the extract on the cells.

Table 6 summarises the absorbance values read from the wells cultured with the Iron/Ti surfaces. The percentage of cell viability calculated with equation 2 was 29.47 ± 0.05% for the treatment with the 304-steel doped with TiO₂ alloy in the form of a porous matrix. These results indicate that of the ~5000 cells seeded per well, for a total of ~15000, only ~1450 survived the treatment.

Table 6. Absorbance measurement in wells cultured with the 304-steel doped with TiO₂ alloy samples doped with 5000sec and 1000sec.

Alloy sample	Reading	Absorbance	Average absorbance per well	Average Total Absorbance
304-steel doped with TiO ₂ alloy doped with 5000 sec	1	0.534	0.547	0.583
	2	0.568		
	3	0.539		
304-steel doped with TiO ₂ alloy doped with 1000 sec	1	0.5653	0.619	
	2	0.6204		
	3	0.6714		

4. DISCUSSION

There are many parameters affecting the quality and performance of plasma spray coating. In this study, it was understood that the production conditions used by DC sputtering magnetron coating can be used in the stainless-steel coating process. The microstructure of the coating samples exhibits the typical morphology of samples coated with the plasma spray method. It is known that the intermediate layer under the main coating layer in the plasma spray process improves the mechanical properties. The intermediate layer is always thinner than the main coating layer (20μm in this study). The powders of the intermediate layer fill the irregularities on the surface of the substrate

material with the flow process under the effect of temperature during the process and create a less rough surface. The powders forming the main coating layer accumulate on the smoothed surface. Thus, a good wetting occurs between the intermediate layer and the primary coating. This event is the occurrence of mechanical bonding between the two layers and increases the mechanical properties of the coating. The results obtained in the experimental studies are based on this statement. In fact, as a result of the coating of stainless steel on the metal with an average surface roughness value of Ra: 7.4 μm and the intermediate layer with an average surface roughness value of Ra: 9.05 μm, Ra: 12.79 μm was found in the direct coating and Ra: 9.92 μm in the coating on the intermediate layer.

The fact that the final surface roughness of the coatings containing the intermediate layer application are lower than the samples directly coated with stainless steel indicates that the two coatings (intermediate layer-main coating) wet each other well. On the other hand, it is stated in the literature that surfaces with low surface roughness positively affect cell growth [20]. According to ISO 10993-5:2009 [Standardization 2009], cytotoxic effects are considered to occur when there is a reduction in cell viability of more than 30% in the biological evaluation of medical devices. According to Table 2, the TiO₂ alloy samples doped with 5000sec and 1000sec used in this work have cytotoxic effects on the CHO cell line. The CHO cell line is characterised by its resistance, fast generation time, ease of handling, and *in vitro* culture. The observed cellular response, in the presence of the alloy and its corrosion products, suggests that other types of alloys should be considered when manufacturing and developing three-dimensional structures that allow cell growth and support bone tissue regeneration. The results show that cell viability is directly influenced by the release of ions from the alloy and indirectly by the variations in pH and osmolality values that these ions produce, given the yellow colouration observed in the treated wells. In addition to considering alloying elements, recent research has shown that for bone tissue engineering applications, the design of three-dimensional scaffolds is necessary, in which the geometry of the porous microstructure becomes a key factor for controlling the mechanical function of the bone-scaffold system, in the tissue regeneration process, as well as after regeneration.

5. CONCLUSIONS

This research aims at developing technical knowledge that supports innovation in the development of biomaterials for the different problems that frequently impede the free development of the community, attenuating along the way the problems generated in the implant by the biological system in terms of biocompatible properties. The general results from the study aiming to coat titanium on a stainless-steel substrate using a plasma spray process can be listed as follows.

- The process parameters used to produce titania doping in the literature can also be used in coating titanium on a 304 stainless steel.
- The powders' surface morphology and grinding method used in the successful coating process are essential parameters.
- For the development of this study, porous structures were manufactured from the 304/TiO₂ alloy, which was used to evaluate the application potential in bone tissue engineering applications and, additionally, the possible cytotoxic effects that can be generated by the biodegradation products of the material once immersed in a biological medium. The results show an appreciable cytotoxic impact on CHO cells, which may be related to the high concentration of metal ions produced by the biocorrosion of the material, which makes a rapid change in the pH of the culture medium, evidenced by its colour change. These findings hint at the necessity for much more thorough research on the behaviour of the alloy in biological media, just as they hint at the necessity of doing similar studies with osteogenic cell lines, which enable the demonstration of bone tissue formation surrounding the magnesium alloy.
- In line with the results obtained, these studies should be evaluated in an *in-vivo* environment in the future.

REFERENCES

- [1] P. J. Kelly and R. D. Arnell, "Magnetron sputtering: a review of recent developments and applications," *Vacuum*, vol. 56, no. 3, pp. 159–172, Mar. 2000, doi: [10.1016/s0042-207x\(99\)00189-x](https://doi.org/10.1016/s0042-207x(99)00189-x).
- [2] A. Baptista, F. Silva, J. Porteiro, J. Míguez, and G. Pinto, "Sputtering Physical Vapour Deposition (PVD) Coatings: A Critical Review on Process improvement and Market Trend Demands," *Coatings*, vol. 8, no. 11, p. 402, Nov. 2018, doi: [10.3390/coatings8110402](https://doi.org/10.3390/coatings8110402).
- [3] M. Braun, "Magnetron sputtering technique," in *Springer eBooks*, 2014, pp. 2929–2957. doi: [10.1007/978-1-4471-4670-4_28](https://doi.org/10.1007/978-1-4471-4670-4_28).
- [4] J. G. Odhiambo, W. Li, Y. Zhao, and C. Li, "Porosity and its significance in Plasma-Sprayed coatings," *Coatings*, vol. 9, no. 7, p. 460, Jul. 2019, doi: [10.3390/coatings9070460](https://doi.org/10.3390/coatings9070460).

- [5] M. I. Boulos, P. L. Fauchais, R. H. Henne, and E. Pfender, "Plasma in the thermal spray coating industry," in *Springer eBooks*, 2022, pp. 1–87. doi: [10.1007/978-3-319-12183-3_35-1](https://doi.org/10.1007/978-3-319-12183-3_35-1).
- [6] R. A. Hammudi et al., "The antimicrobial activity of (DBD) homemade plasma jet against *Staphylococcus aureus* using different gases," *Advanced Engineering Science*, vol. 54, iss. 3, May, 2022.
- [7] J. Arun, S. Nachiappan, G. Rangarajan, R. P. Alagappan, K. P. Gopinath, and E. Lichtfouse, "Synthesis and application of titanium dioxide photocatalysis for energy, decontamination and viral disinfection: a review," *Environmental Chemistry Letters*, vol. 21, no. 1, pp. 339–362, Aug. 2022, doi: [10.1007/s10311-022-01503-z](https://doi.org/10.1007/s10311-022-01503-z).
- [8] R. Li, T. Li, and Q. Zhou, "Impact of Titanium Dioxide (TiO₂) Modification On Its Application to Pollution Treatment—A Review," *Catalysts*, vol. 10, no. 7, p. 804, Jul. 2020, doi: [10.3390/catal10070804](https://doi.org/10.3390/catal10070804).
- [9] X. Fu et al., "The optimized preparation of HA/L-TiO₂/D-TiO₂ composite coating on porous titanium and its effect on the behavior osteoblasts," *Regenerative Biomaterials*, vol. 7, no. 5, pp. 505–514, May 2020, doi: [10.1093/rb/rbaa013](https://doi.org/10.1093/rb/rbaa013).
- [10] K. H. Lo, D. Zeng, and C. T. Kwok, "Effects of sensitisation-induced martensitic transformation on the tensile behaviour of 304 austenitic stainless steel," *Materials Science and Engineering A*, vol. 528, no. 3, pp. 1003–1007, Oct. 2010, doi: [10.1016/j.msea.2010.09.060](https://doi.org/10.1016/j.msea.2010.09.060).
- [11] V. Vancoppenolle, P. -y. Jouan, M. Wautelet, J. -p. Dauchot, and M. Hecq, "D.c. magnetron sputtering deposition of TiO₂ films in argon-oxygen gas mixtures: theory and experiments," *Surface and Coatings Technology*, vol. 116–119, pp. 933–937, Sep. 1999, doi: [10.1016/s0257-8972\(99\)00267-4](https://doi.org/10.1016/s0257-8972(99)00267-4).
- [12] M. A. Ulkareem, F. T. M. Noori, and M. K. Khalaf, "Corrosion resistance of Ti6Al4V alloy by Radio Frequency Technique used for Coating Deposition of multilayer (HA/TiN/Ti6Al4V-substrate) for Optimization power," *IOP Conference Series Materials Science and Engineering*, vol. 757, no. 1, p. 012047, Mar. 2020, doi: [10.1088/1757-899x/757/1/012047](https://doi.org/10.1088/1757-899x/757/1/012047).
- [13] R. A. Hammudi et al., "Plasma in dentistry," *Malaysian Journal of Fundamental and Applied Sciences*, vol. 19, no. 3, pp. 332–336, May 2023, doi: [10.11113/mjfas.v19n3.2904](https://doi.org/10.11113/mjfas.v19n3.2904).
- [14] K. H. S. Main, J. I. Provan, P. J. Haynes, G. Wells, J. A. Hartley, and A. L. B. Pyne, "Atomic force microscopy—A tool for structural and translational DNA research," *APL Bioengineering*, vol. 5, no. 3, Jul. 2021, doi: [10.1063/5.0054294](https://doi.org/10.1063/5.0054294).
- [15] H. A. Colorado, H. R. Salva, H. R. Salva, A.A. Ghilarducci, "Residual elastic strain of aisi 304 stainless steel sheets covered with a titanium nitride thin film deposited by pvd-magnetron sputtering," *Dyna*, vol. 76, no. 160, pp. 207–21, 2009.
- [16] W.-J. Chou, G.-P. Yu, and J.-H. Huang, "Mechanical properties of TiN thin film coatings on 304 stainless steel substrates," *Surface and Coatings Technology*, vol. 149, no. 1, pp. 7–13, Jan. 2002, doi: [10.1016/s0257-8972\(01\)01382-2](https://doi.org/10.1016/s0257-8972(01)01382-2).
- [17] R. Ghanem et al., "Effect of Ti doping on the structural, morphological and magnetic properties of La_{0.7}Ga_{0.3}Fe_{1-x}Ti_xO₃," *Results in Physics*, vol. 26, p. 104342, May 2021, doi: [10.1016/j.rinp.2021.104342](https://doi.org/10.1016/j.rinp.2021.104342).
- [18] A. Oyane, H. Kim, T. Furuya, T. Kokubo, T. Miyazaki, and T. Nakamura, "Preparation and assessment of revised simulated body fluids," *Journal of Biomedical Materials Research Part A*, vol. 65A, no. 2, pp. 188–195, Mar. 2003, doi: [10.1002/jbm.a.10482](https://doi.org/10.1002/jbm.a.10482).
- [19] L. L. Hench and J. Wilson, *An introduction to bioceramics*. 1993. doi: [10.1142/2028](https://doi.org/10.1142/2028).
- [20] D. Campoccia, "In vitro behaviour of bone marrow-derived mesenchymal cells cultured on fluorohydroxyapatite-coated substrata with different roughness," *Biomaterials*, vol. 24, no. 4, pp. 587–596, Dec. 2002, doi: [10.1016/s0142-9612\(02\)00373-3](https://doi.org/10.1016/s0142-9612(02)00373-3).